MYC oncogene is associated with suppression of tumor immunity and targeting Myc induces tumor cell immunogenicity for therapeutic whole cell vaccination

Xiaofang Wu [1], Marie Nelson,[1] Mousumi Basu,[1] Priya Srinivasan,[1] Christopher Lazarski,[2] Peng Zhang,[3] Pan Zheng,[3] Anthony David Sandler [1,4]

Correspondence to
Dr Anthony David Sandler; asandler@childrensnational.org

ABSTRACT

Background MYC oncogene is deregulated in 70% of all human cancers and is associated with multiple oncogenic functions including immunosuppression in the tumor microenvironment. The role of MYC in the immune microenvironment of neuroblastoma and melanoma is investigated and the effect of targeting Myc on immunogenicity of cancer cells is evaluated.

Methods Immune cell infiltrates and immunogenic pathway signatures in the context of MYCN amplification were analyzed in human neuroblastoma tumors and in metastatic melanoma. Dose response and cell susceptibility to MYC inhibitors (I-BET726 and JQ1) were determined in mouse cell lines. The influence of downregulating Myc in tumor cells was characterized by immunogenic pathway signatures and functional assays. Myc-suppressed tumor cells were used as whole cell vaccines in preclinical neuroblastoma and melanoma models.

Results Analysis of immune phenotype in human neuroblastoma and melanoma tumors revealed that MYCN or c-MYC amplified tumors respectively are associated with suppressed immune cell infiltrates and functional pathways. Targeting Myc in cancer cells with I-BET726 and JQ1 results in cell cycle arrest and induces cell immunogenicity. Combining vaccination of Myc-inhibited tumor cells with checkpoint inhibition induced robust antitumor immunity and resulted in therapeutic cancer vaccine therapy in mouse neuroblastoma tumors. Despite vigorous antitumor immunity in the mouse melanoma model, upregulation of immunosuppressive pathways enabled tumor escape.

Conclusions This study demonstrates that the Myc oncogene is an appropriate target for inducing tumor cell immunogenicity and suggests that Myc-suppressed whole tumor cells combined with checkpoint therapy could be used for formulating a personalized therapeutic tumor vaccine.

INTRODUCTION

The need for more effective therapy of tumors like neuroblastoma and melanoma is evident in the poor outcome of high-risk or advanced disease. Cancer vaccines and immune-based therapies hold great promise for malignant solid tumors, but despite robust immune activation with targeted checkpoint inhibitors, cure is often elusive especially in non-immunogenic tumors. Immune-based therapies (and specifically tumor vaccines) are constrained by antigen selection due to the high diversity of tumor antigens across patient tumors and also by intrinsic tumor cell mechanisms enabling tumor immune privilege/evasion. The ability to develop a personalized tumor vaccine combined with blockade of immune privilege mechanisms could circumvent these constraints.

Amplification of the Myc oncogene is associated with immune privilege.[1–3] Our recent in silico analysis of neuroblastoma showed the association of repressed cellular immunity within MYCN-amplified tumors.[1] In the current study, neuroblastoma tumors underwent immune phenotyping by examining immune cell infiltrates and immunogenic pathway signatures in the context of MYCN amplification. Immune cell infiltrates were suppressed in MYCN-amplified tumors and similarly, analysis of cell lines also displayed complete suppression of immunogenic pathways in MYCN-amplified cells. MYCN-amplified high-risk neuroblastoma failed to respond to checkpoint inhibitor therapy in preliminary trials[4] that may be explained by the inability to engage host immunity. Host immunity and tumor-specific immune cells in the tumor bed are essential for effective checkpoint immunotherapy.

MYC oncogenes appear to play a role in immunogenicity by creating an environment of immune privilege for the tumors themselves. MYC proteins including MYCN, c-MYC

and MYCL are critical in tumorigenesis and are implicated in oncogenic pathways in 70% of human cancers.[5] Several groups have worked on targeting MYC with small molecule inhibitors,[6–10] however no clinical stage molecules are as yet available. These molecules either directly bind to and inhibit MYC activity or disrupt the MYC/MAX dimerization.[7 11–15] Epigenetic modifiers that target the bromodomains by recognizing acetylated lysine residues are of particular interest as these will reprogram tumor cells and alter transcription machinery. Applying these drugs in vitro to cell culture enables modification of the tumor cells without the need for clinical grade inhibitors. Furthermore, the in vitro use of these drugs to modify cancer cells directly averts the potential side effects of systemic clinical use. We thus hypothesized that direct inhibition of MYC function in tumor cells would create an immunogenic phenotype that would circumvent antigen selection and immune privilege/ evasion in development of a whole cell vaccine strategy.

Mouse neuroblastoma and melanoma cell lines were tested for their susceptibility to Myc targeting. Dose response testing was performed with highly specific Bromodomain inhibitors I-BET726 and JQ1, to determine suppression of Myc oncogenes. Treatment of whole tumor cells suppressed Myc-n and c-Myc expression and induced cell cycle arrest with a differentiated phenotype. These pharmacologic Myc inhibitors upregulated immunogenic cell pathways involved in antigen processing and immune activation. The treated cell lines induced tumor cell immunogenicity stimulating host immunity as detected by multiplex proinflammatory cytokine and chemokine secretion. We subsequently tested tumor immunity when Myc -targeted cells were administered as whole cell vaccines in combination with checkpoint inhibitors in established mouse tumor models. Irradiated Myc-targeted tumor cells induced robust tumor immunity in mouse neuroblastoma and melanoma models, in which the vaccine strategy was markedly effective in curing established neuroblastoma tumors. Targeting Myc in tumor cells serves as a relatively simple and effective means for creating a personalized immunogenic whole cell vaccine when combined with checkpoint inhibitors.

METHODS
Human neuroblastoma samples
Human tumor specimens were obtained from 21 patients diagnosed with low-risk (n=4), intermediate-risk (n=6), and high-risk (n=11) neuroblastoma of which 5 were MYCN amplified. Diagnosis and staging were performed according to Children's Oncology Group (COG) risk stratification. Biopsies or tumor resection were performed at time of diagnosis and prior to initiation of therapy as part of clinical care. Specimen collection for research purposes of this study was obtained after completion of appropriate consents and assents and was approved by the Institutional Review Board, Children's National Hospital, Washington, DC (Pro00004284, Pro00009692). Archival tissue

samples with known risk-stratification, MYCN status, and outcome data were made available through IRB-approved protocol Pro00009594.

Human melanoma samples
We audited the largest publicly available cancer genomic database, namely, The Cancer Genome Atlas (TCGA) with genomic, transcriptomic, and clinical data for human metastatic melanoma (SKCM-TM) samples. The clinical data of cancer samples were accessed from the cBioPortal for Cancer Genomics database (http://www.cbioportal.org/index.do (cbioportal.org), February 2020). The mRNA expression quantification profiles based on the RNA sequencing and copy number variation status for each gene were downloaded from the TCGA data portal (https://portal.gdc.cancer.gov/ (portal.gdc.cancer.gov), February 2020). A total of 354 human metastatic melanoma samples (with copy number variation status is 'Amplification' or 'Diploid') were kept for further analysis.

Animals
Female C57BL/6 and A/J mice aged 6 weeks were purchased from Jackson Laboratories (Bar Harbor, Maine, USA). All procedures were approved by the Institutional Animal Care and Use Committee (IACUC) of Children's National Medical Center, Washington, DC.

Cells
The murine melanoma B16-F10 cell line (ATCC, Manassas, Virginia, USA) and mouse neuroblastoma Neuro2a cell line (Sigma, St. Louis, Missouri, USA) were cultured using DMEM supplemented with 10% heat-inactivated fetal bovine serum (FBS, Sigma) and 100 IU/mL penicillin, 100 µg/mL streptomycin. Human neuroblastoma SK-N-SH (MYCN non-amplified, Sigma) and IMR-32 (MYCN amplified) cells (Sigma) were cultured in EMEM supplemented with 2 mM glutamine, 1% non-essential amino acids, 10% FBS and 100 IU/mL penicillin, 100 µg/mL streptomycin. All media and supplement were purchased from Thermo Fisher Scientific (Waltham, Massachusetts, USA).

Antibodies and reagents
Anti (α)-mouse CTLA-4, α-mouse programmed death-ligand 1 (PD-L1), and mouse IgG2b isotype antibodies were purchased from BioXCell (West Lebanon, New Hampshire, USA). Mouse Ki67 Alexa Fluor 647, PD-1 PE, GR-1(Ly6G/Ly6C) Brilliant Violet 650, DX5 Dazzle 594, CD11c PE/Cy7, LAG3 Brilliant Violet 650, TIM3 PE/Cy7, CD3e PerCP/Cy5.5, CD11b FITC, CD45 APC/Fire 750, α-CD4 Brilliant Violet 421 and α-CD8a Brilliant Violet 605 were bought from BD Biosciences (San Jose, California, USA). Mouse F4/80 Superbright 702, FoxP3 PE and nestin monoclonal antibodies were purchased from Thermo Fisher. I-BET726 was purchased from Millipore Sigma (Burlington, Massachusetts, USA) and JQ1 was purchased from Tocris (Minneapolis, Minnesota, USA).

Live/dead fixable aqua dead cell stain kit and Brilliant stain buffer were purchased from Thermo Fisher.

Splenocyte IFNγ assay

A total of 5×10^5 splenocytes were cocultured with 5×10^4 B16 cells for 24 hours or 48 hours. Supernatants were collected from triplicate wells, and IFNγ was assayed using the mouse uncoated IFNγ ELISA kit from Invitrogen (Carlsbad, California, USA). Readings were measured at 450 nm using the EnSpire 2300 Multilabel plate reader (Perkin Elmer, Waltham, Massachusetts, US).

Multiplex cytokine/chemokine analysis

The concentrations of cytokines and chemokines were determined using the mouse 36-plex ProcartaPlex Panel (Thermo Scientific). Briefly, cell culture supernatant samples were mixed with antibody-linked polystyrene beads on a 96-well plate and incubated at room temperature (RT) for 2 hours. After washing, plates were incubated with biotinylated detection antibody for 30 min at RT. The labeled beads were resuspended in streptavidin-PE for 30 min at RT, each sample was measured in duplicate along with standards (8-point dilutions) and the buffer control. Plates were read using a Luminex Bioplex 200 system (Bio-Rad, Hercules, California, USA).

Nanostring immune profiling in neuroblastoma

RNA was extracted from tumor tissue and cells using Purelink RNA mini kit (Thermo Fisher Scientific) per standard techniques. RNA was extracted from the formalin-fixed paraffin embedded (FFPE) human tumor samples through use of the MagMAX FFPE DNA/RNA Ultra Kit (Applied Biosystems). Gene expression was directly measured via counts of corresponding mRNA in each sample using an nCounter PanCancer Immune Profiling Panel (NanoString, Seattle, Washington, USA), which includes 770-plex gene expression panel covering innate and adaptive immune responses, that include T and B cell activation and inhibition, inflammation, adhesion molecules, chemokines and cytokines, and pattern recognition receptors.[16][17] According to the manufacturer's instructions, 100 ng of high-quality total RNA was hybridized with reporter probes and biotinylated capture probes at 65°C for 16–18 hours before being placed into the nCounter Prep station in which samples were affixed to a cartridge. Cartridges were then read by the nCounter Digital Analyzer optical scanner (Nanostring Technologies, Washington, USA). Further advanced immune-profiling analysis was performed using nSolver V.4.0 analysis software (NanoString Technologies).

Infiltrating immune cell abundance estimation in melanoma

We used the tumor immune estimation resource (TIMER, http://timer.cistrome.org/ (timer.cistrome.org)) framework to estimate the abundance of different immune cell phenotypes in the tumor microenvironment based on the transcriptome data of human metastatic melanoma samples. Specifically, we employed the TIMER webserver to calculate the abundances of six immune infiltrates (B cells, CD4 T cells, CD8 T cells, neutrophils, macrophages, and dendritic cells (DCs)) based on the gene expression matrix of each TCGA cancer sample derived from RNA sequencing data with the selection of corresponding cancer type.

Real-time reverse transcription - polymerase chain reaction (RT-PCR)

RNA was extracted using Purelink RNA mini kit (Life Technologies) per standard techniques. Real-time PCR was performed using TaqMan Gene Expression Master Mix (Life Technologies) in a QuantStudio 7 Flex Real-Time PCR System (Thermo Fisher Scientific), according to the manufacturer's instructions. Each of the reactions was performed in triplicate, including no template controls and amplification of a housekeeping gene, GAPDH. Gene-specific assays were Mm00452054_m1 for mouse PD-L1, Mm00803857_m1 for mouse n-myc, Mm00487804_m1 for mouse c-myc, Mm00775963_g1 for mouse Id1, Mm00711781_m1 for mouse Id2, Mm00492575_m1 for mouse Id3, Mm00499701_m1 for mouse Id4, Mm99999915_g1 for mouse Gapdh, Hs00232074_m1 for human MYCN, Hs00153408_m1 for human c-MYC, Hs00204257_m1 for human PD-L1 and Hs02786624_g1 for human GAPDH (Life Technologies). Changes in relative gene expression normalized to GAPDH levels were determined using the ΔΔCt method. Results were averaged and statistically analyzed using t-tests.

Western blot analysis

Cells were lysed in RIPA lysis buffer containing protease inhibitors (Roche, Indianapolis, Indiana, USA) on ice. After centrifuging at maximum speed for 15 min at 4°C, the supernatant protein concentration was estimated by BCA protein assay (Pierce, Rockford, Illinois, USA) according to manufacturer's instruction. Forty micrograms of proteins were loaded per well for electrophoresis on NuPAGE Novex 4%–12% Bis-Tris gels (Invitrogen, Carlsbad, California, USA), after which the proteins were transferred to a nitrocellulose membrane (Invitrogen) and blocked with 5% milk. The blots were incubated overnight with goat anti-mouse PD-L1 antibody (1:200, R&D, Minneapolis, Minnesota, USA), rabbit anti-mouse c-Myc antibody (1:1000, abcam, Cambridge, Massachusetts, USA), rabbit anti-mouse n-Myc (1:500, abcam), rabbit anti-human MYCN antibody (1:1000, cell signaling), goat anti-human c-myc antibody (1:400, R&D), and goat anti-human PD-L1 antibody (1:100, R&D), followed by HRP-conjugated secondary antibody (1:2000, Santa Cruz, Dallas, Texas, USA). Blots were developed by chemiluminescence using the SuperSignal Kit (Thermo Fisher, Waltham, Massachusetts, USA). Mouse anti vinculin antibody (1:1000, Santa Cruz) was used as a control for protein loading variations.

Mouse tumor therapeutic models

As described previously,[2][18] for the melanoma model C57BL/6 mice were injected subcutaneously in the right

flank with 1×10^4 freshly prepared B16 wild-type (wt) tumor cells on day 0. For vaccination, 1×10^6 Myc inhibitor treated and irradiated (60 Gy) B16 cells and TLR7/8 agonist (25 μg/mouse) was injected (subcutaneously) into the left flank of each mouse on day 4, 11 and 18 as a whole tumor cell vaccine along with anti-CTLA-4 and anti-PD-L1 (100 μg/mouse) administered intraperitoneally. TLR7/8 agonist was used in an attempt to enhance immunity induced by the vaccine. This was not considered to be necessary in the neuroblastoma model in which a high cure rates were observed. For the neuroblastoma model, the right flanks of A/J mice were injected (subcutaneously) with 2×10^6 Neuro2a cells on day 0. For vaccination, Myc inhibited and irradiated (40 Gy) Neuro2a cells or untreated/irradiated (40 Gy) Neuro2a cells were injected (subcutaneously) into the left flank on day 7 and 12. Anti-CTLA-4 and anti-PD-L1 (100 μg/mouse) was administered (intraperitoneally.) on day 7, 9 and 12. Mice were monitored daily following tumor inoculation and tumor growth was recorded in two dimensions. Tumor volume was calculated using the following formula: largest diameter^2 × smaller diameter × 0.52. A tumor size of 20 mm in any dimension was designated as the endpoint, and mice were euthanized at that time. All the procedures are approved by the IACUC at Children's National Hospital and are in accordance with the humane care of research animals.

Flow cytometry of tumor-infiltrating lymphocytes (TILs)

1×10^4 wt B16 melanoma cells were injected into the right leg of C57BL/6 mice on day 0. On day 7, 10 and 13, 1×10^6 whole tumor cell vaccines and TLR7/8 (25 μg/mouse) were injected into the left leg of mice, combined with intraperitoneal administration of anti-CTLA-4 and anti-PD-L1. Tumor, spleen and tumor draining lymph nodes as well as nodes from the contralateral side were excised on day 15, when one dimension of tumor diameter reached 5–8 mm, and on day 22 when tumors reach about 10–14 mm. Tissue was meshed through a 40 μm strainer and 1×10^6 single cells were incubated in 100 μL Live Dead Viability Dye for 25 min at 4°C. After three washes, two sets of staining were performed. For staining cell surface markers, cells were incubated for 30 min at 4°C with the following conjugated antibodies: CD3 PerCP Cy5.5, CD4 Brilliant Violet 421, CD8 Brilliant Violet 605, CD45 APC fire 750, CD11b FITC, CD11c PE cy7, DX5 PE/dazzle 594, Tim3 PE/Cy7, LAG3 Brilliant Violet 650 and GR1 Brilliant Violet 650. For staining intracellular markers, cells were fixed in 1× fixation solution for 25 min at 4°C and then resuspended in 1× CytoFix/Cytoperm buffer containing conjugated Ki67 (1:200) or Foxp3 (1:100) antibodies at 4°C for 20 min. Appropriate isotype antibodies were used as negative controls. Samples were run on a Calibur-DxP platform (Cytek Biosciences). Data were analyzed using FlowJo V.10.0.5 (Treestar, Ashland, Oregon).

Characterization of Neuro2a cells by immunofluorescent staining

Neuro2a cells were fixed in 4% paraformaldehyde (Sigma) for 15 min. Immunofluorescence staining was performed as previously described[2 18] using the primary nestin mouse monoclonal (mAb, 1:100, Thermo Fisher). Isotype-matched antibodies were used for negative controls. All fluorescent images were acquired with a Zeiss LSM 510 confocal microscope (Carl Zeiss MicroImaging, Thornwood, New York, USA). Images were taken at magnifications of 630× under oil immersion.

Statistical analysis

Statistical analysis of gene expression, normalization, quality control, clustering, Pathview plots, fold-changes and statistical ranking of differentially expressed genes were performed using the Advanced Analysis Module in the nSolver Analysis Software V.4.0 from NanoString Technologies (NanoString Technologies). Raw data for each sample were normalized to the geometric mean of endogenous housekeeping genes using the geNorm algorithm. Pathway scores are calculated as the first principal component of the pathway genes' normalized expression. Each cell type score has been centered to have mean 0 and as abundance estimates (cell type scores) are calculated in log2 scale, an increase of 1 corresponds to a doubling in abundance. All differentially expressed genes were subjected to KEGG term analysis, with significance accepted at $p < 0.05$. The Benjamini-Yekutieli method was used to control the false discovery rate. All statistical analyses of nanostring data were carried out in R V.3.4.3 software.

The specific tests used to analyze each set of experiments are indicated in the figure legends. The data are expressed as the mean (±SD) and analyzed using an unpaired two-tailed Student's t-test for comparisons between two groups, with $p < 0.05$ considered statistically significant. A non-parametric Wilcoxon rank-sum test was used when comparing the association between MYC amplification and tumor immunity in TCGA metastasis melanoma samples.

RESULTS

MYCN amplification in human neuroblastoma and c-MYC amplification in melanoma tumors are associated with suppressed expression of genes and pathways related to immunity

Amplification of MYCN is shown to correlate with poor prognosis in patients,[19 20] a biomarker that is key to clinical risk stratification. In an in silico study of 148 neuroblastoma tumors, we previously found a significant reduction in most immune cell subsets in MYCN-amplified human neuroblastoma tumors.[1] To further investigate the role of MYCN amplification in immunity, we assessed immune gene profiling using the mRNA Pan-Cancer Immune Profiling Panel (NanoString nCounter system) in 21 risk-stratified neuroblastoma tumors. This 770-plex assay
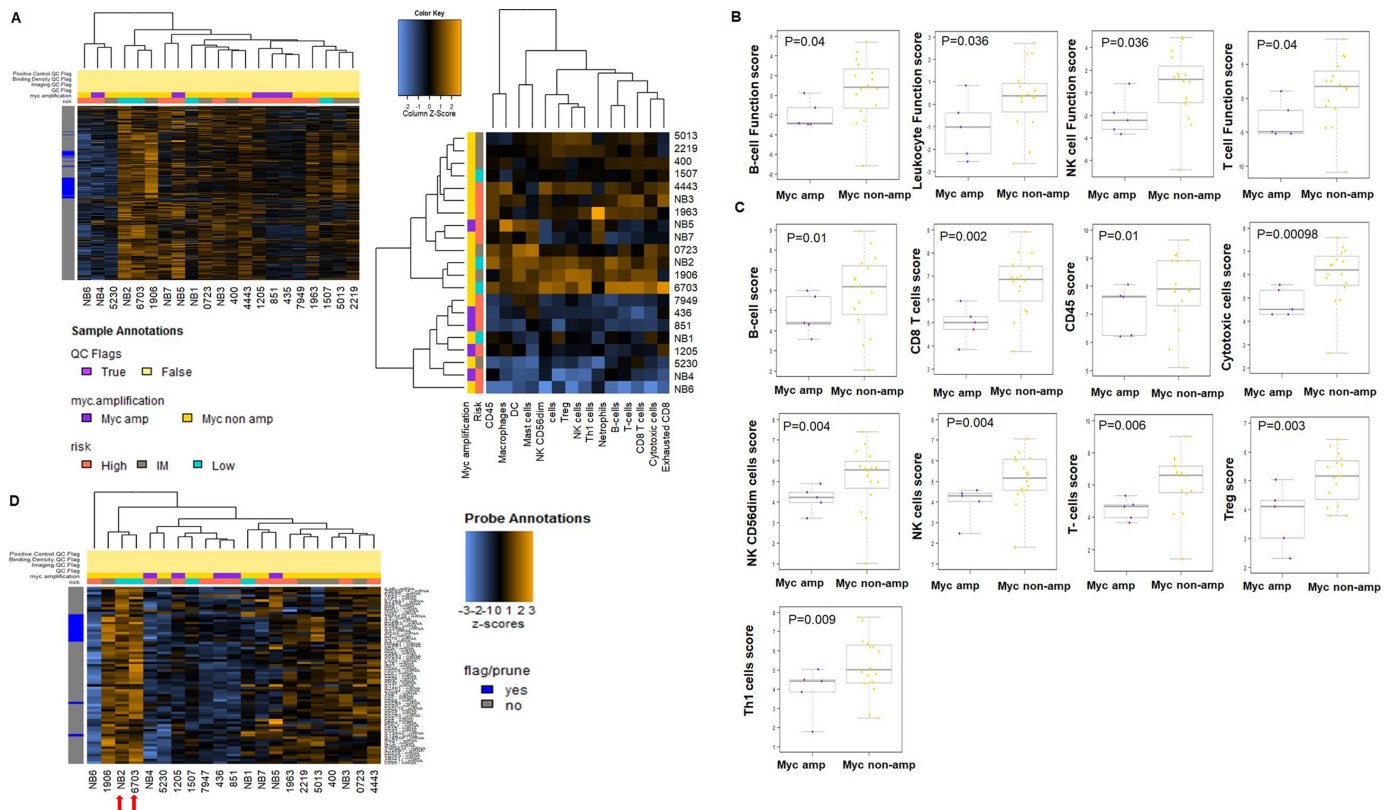
Figure 1 MYCN-amplification in human neuroblastoma is associated with significantly depressed immune cell infiltrate and function score. (A) Heat map in left panel shows hierarchical immune gene expression clustering of human neuroblastoma samples (n=21). MYCN-amplified samples (purple) generally clustered together from MYCN non-amplified samples, except for NB4 and NB5. The heat map on the right panel shows immune gene clustering of human neuroblastoma samples based on cell type signature scores. Again, NB5 clustered furthest from the group of MYCN-amplified samples. (B) Immune cell function is significantly lower in MYCN-amplified neuroblastoma. Box plots of gene expression signature scores of human neuroblastoma for genes involved in B cell, leukocyte, NK cell, and T cell function are shown distinguishing MYCN amplified (n=5) from non-amplified (n=16) human neuroblastoma samples. (C) Immune cell number is decreased in MYCN-amplified neuroblastoma. Box plots showing distribution of immune cells by relative number present within human neuroblastoma samples calculated by gene expression. CD45+ (immune cell marker), B cells, T cells (CD8+, Treg, Th1 cells) and NK cells were significantly reduced in MYCN-amplified versus non-amplified samples (p<0.05). As abundance estimates (cell type scores) are calculated in log2 scale, an increase of 1 on the vertical axis corresponds to a doubling in abundance. The horizontal black line on the box plot represents the median expression. Statistical significance was determined by unpaired two-tailed Student's t-test (p<0.05). (D) Heat map showing clustering based on expression of genes important to T cell function that is prevalent in lower risk, MYCN non-amplified samples. Tumor samples from patients with OMAS, which are at low risk for disease recurrence and present with an associated immunogenic paraneoplastic syndrome, are designated with red arrows. NK, natural killer; OMAS, opsoclonus-myoclonus-ataxia syndrome; Treg, regulatory T cells.

contains 109 genes related to cell surface markers capable of quantifying 14 different tumor-infiltrating immune cell types, 30 genes for commonly studied CT antigens and over 500 genes indicating immune response.[16 17]

The clinical data of the 21 patient samples collected are shown in online supplemental table S1. A majority of patients had metastatic disease at diagnosis (n=9). Two low-risk samples were collected from patients with associated opsoclonus-myoclonus-ataxia syndrome (OMAS). Gene expression from mRNA extracted from human tumors was measured using the nCounter PanCancer Immune Profiling Panel and comparisons made between MYCN amplified and non-amplified tumors. Figure 1A (left) shows the results of unsupervised hierarchical clustering of the mean values of all immune genes expressed

while figure 1A (right) shows the heat map of pathway scores.

Overall, there was a significant reduction in multiple signature pathway scores in MYCN-amplified tumors when compared with MYCN non-amplified tumors, most distinctly seen in T cell function, but also noted in B cell function, natural killer (NK) function, antigen-processing, cytotoxicity, cytokine and chemokine signatures (figure 1B). Further, decreased presence of immune cells were measured in MYCN-amplified tumors, including T cells (CD8+ cells included), NK cells and B cells (figure 1C). Low-risk tumors associated with OMAS (n=2) that have an excellent survival were a particularly immunogenic subtype with regard to T cell function (NB2 and FFPE 6703, figure 1D). A few patients

had immune gene signatures that did not clearly fit the MYCN amplification paradigm. NB5, a high-risk MYCN-amplified tumor was an outlier in this assessment as the tumor had a higher T cell function score similar to the intermediate-risk tumors. This patient survived through induction chemotherapy, surgical resection, radiation to primary tumor site and received single autologous stem cell transplant HSCT per standard of care at that time. Unfortunately, this patient passed away during cycle 2 of immunotherapy with dinutuximab (chimeric 14.18 antibody) and interleukin-2 (IL-2) due to adenoviral infection and acute respiratory distress syndrome and not recurrent disease. NB6, a high-risk MYCN non-amplified tumor was from a 6-year-old male who presented with widely metastatic disease, and was treated as per COG high-risk standard protocol with induction chemotherapy, surgical resection of primary tumor, radiation, and tandem (x2) autologous HSCT. At this time, he is just over a year off therapy without signs of recurrence. The tumor had very low immunogenicity based on gene profiling results, thus genes other than MYCN most likely suppress immune pathways as well. The tumor 5230 was an intermediate-risk, MYCN non-amplified tumor from a patient who was 6 months old at diagnosis and presented with metastatic disease. She was treated with eight cycles of intermediate-risk chemotherapy, and is now 5 years off therapy without signs of disease. This tumor also had low immunogenicity and T cell function based on profiling scores that would not be expected for a lower risk tumor without MYCN amplification. A similar tumor in an older patient (>18 months) would be high-risk, but age under 18 months alone in neuroblastoma is a good prognostic determinant. Despite these patients whose findings seemed to be outliers based on tumor immunity profiling, our findings confirm that globally, MYCN-amplified tumors have a suppressed immunogenic phenotype when compared with non-amplified counterparts, and this immunosuppressive microenvironment is evident across multiple immune pathways present within the tumor, but most markedly in T cell function and CD8+ T cell number. The top 20 genes with differences in expression (p value <0.05) and the top 20 genes altered in T cell function between MYCN non-amplified human neuroblastoma tumors compared with MYCN-amplified tumors are listed in online supplemental tables S2 and S3.

These findings prompted us to evaluate whether MYCN amplification also alters immunogenicity in cultured neuroblastoma cell lines. For this purpose, we compared global immune transcriptome profiles of four human neuroblastoma cell lines, SK-N-SH and SK-N-F1, two MYCN-non-amplified cell lines, and IMR32 and BE(2)C, two MYCN-amplified cell lines. Unsupervised clustering of 750 immune genes shows a strong association with MYCN amplification status (figure 2A). A clear separation of immune pathway activity is observed in the heat map of pathway scores (figure 2B), in which we found a significant and dramatic reduction in the signature scores of multiple immune pathways including antigen

processing, CT antigen, cytokines, chemokines, compliment, interleukins, TLR and TNF superfamily in the MYCN-amplified cell lines compared with MYCN-non-amplified cell lines (figure 2C and D). These observations again confirm that MYCN amplification is associated with repressed cellular immunity. Similar to patient tumors, the MYCN-amplified IMR32 and BE(2)C cell lines have low levels of both immunostimulatory and immunosuppressive genes associating MYCN amplification with globally suppressed immunity. Within the suppressive gene list examined (online supplemental table S4), Annexin A1 (ANXA1) decreased 5540 fold (p value=2.12E–08), Tyrosine-protein kinase receptor (AXL) decreased 505 fold (p value=3.68E–07), and apolipoprotein E (APOE) decreased 61.5 fold (p value=0.000014). PD-L1 decreased 69.8 fold (p value=5.43E–06) and VEGF decreased 38.7 fold (p value=0.0247). MYCN amplification in neuroblastoma is thus strongly associated with an immune-suppressed phenotype and potentially targeting MYC expression may reverse this phenotype.

To determine whether MYC amplification is also associated with repressed immunogenicity in melanoma, we compared the RNA-seq dataset of metastatic melanoma from the TCGA database. A total of 354 patients with melanoma (MYC amplified n=30, MYC non-amplified n=324) were included based on availability of detailed RNA-seq FPKM (Fragments Per Kilobase of transcript per Million mapped reads) data, survival time after diagnosis, risk assignment, and c-MYC-amplification status. The patients with or without MYC amplification are similar in age at diagnosis, gender distribution (online supplemental table S5). As shown in figure 3, MYC-amplified melanoma had significantly lower levels of CTLA-4, PD-L1, CD4 T cell transcripts when compared with MYC non-amplified melanoma, indicating reduced immune response in MYC amplified melanoma and also confirming the data from the neuroblastoma study in which MYCN amplification is associated with suppression of PD-L1 expression. To determine whether MYC effects specific subset of leukocytes, we used immune cell fraction estimation analysis to calculate the percentage of each leukocyte subset. Results showed that macrophages, neutrophils and myeloid DCs were significantly reduced in MYC-amplified tumors. These data suggest that c-MYC amplification in melanoma is also associated with a suppressed host immune response, however the impact appears less profound than that of MYCN amplification in neuroblastoma.

Targeting Myc attenuates proliferation of tumor cells and leads to growth arrest

To determine the effect of Myc targeting on tumorigenesis, we treated mouse neuroblastoma Neuro2a cells and melanoma B16 cells in culture with two Myc inhibitors including I-BET726 and JQ1.[6 7 21 22] In this study, Neuro2a or B16 cells were exposed to different concentrations and/or combinations of I-BET726 and JQ1 and assessed at 3, 4, 5, 7 and 10 days. As demonstrated in figure 4, the combination of I-BET726 at
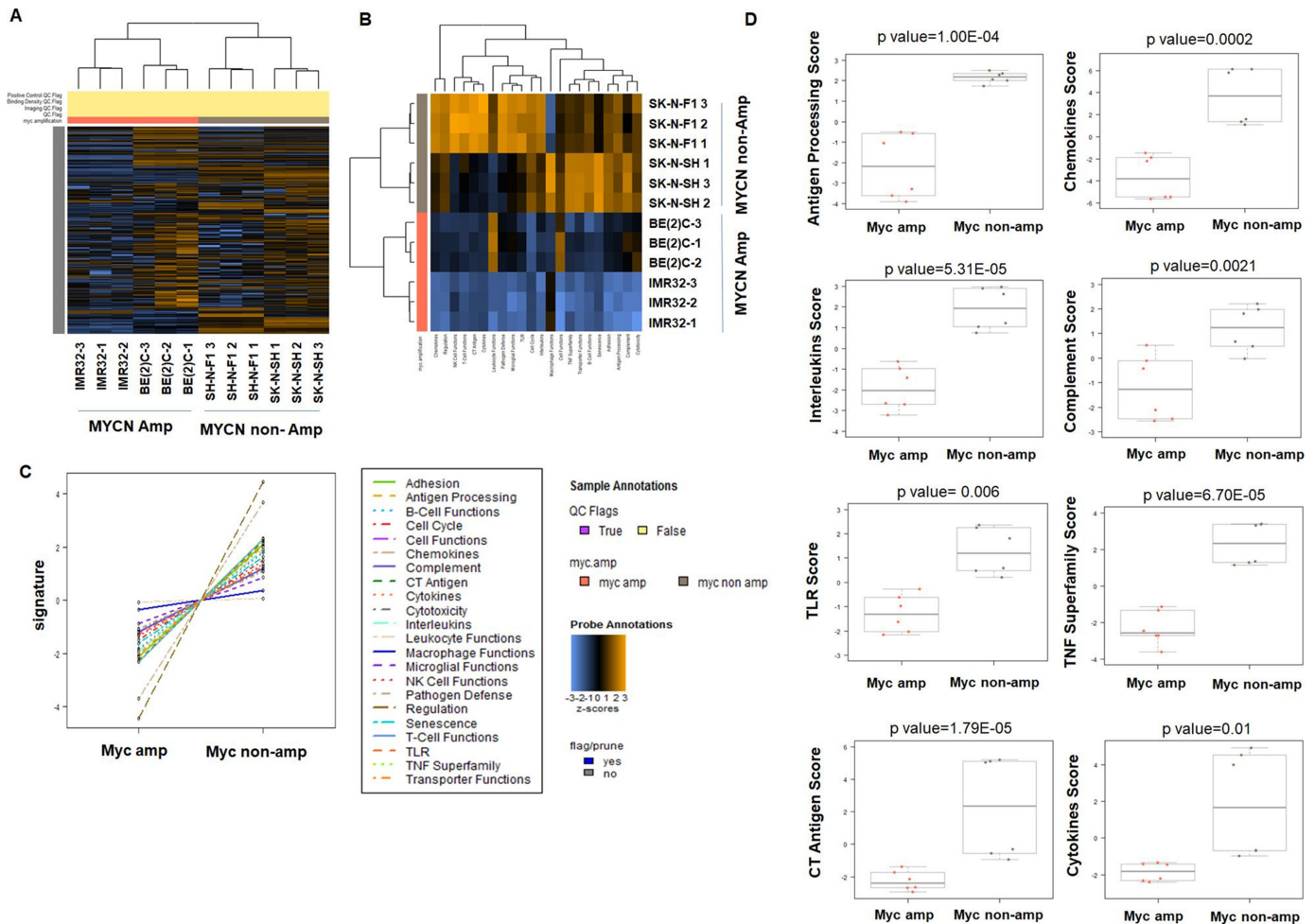
Figure 2 Immune gene expression comparing MYCN-amplified and MYCN-non-amplified human neuroblastoma cell lines. (A) Unsupervised hierarchical clustering of six independent cultured cell samples: SK-N-SH (n=3) and IMR32 (n=3) by expression levels of 750 immune genes. Each row of the heat map is a single probe, and each column is a single sample. The bar at the top denotes MYCN amplification status, with orange=amplified, gray=non-amplified. (B) Heat map of pathway scores, pathways are listed on the horizontal axis and samples are listed vertically. Orange indicates high scores; blue indicates low scores. Scores are displayed on the same scale via a Z-transformation. Clear separation of pathway activity is observed associated with MYCN-amp and MYCN-non-amp cells. (C) Trend dot-line plots of 22 known immune pathways show that they are differentially expressed between MYCN amplified versus non-amplified cells. (D) Box plots of significantly increased pathway scores in SK-N-SH versus IMR32, with median expression. The maximum and minimum expression level is represented by the upper and lower error bars, respectively. Unpaired two-tailed Student's t-test was performed for the statistical analysis (p<0.05).

0.25 μM and JQ1 at 0.25 μM for 4 days followed by irradiation (60 Gray) produced complete suppression of Myc genes and its downstream pathways, including Id genes and PD-L1 in both B16 (figure 4A) and Neuro2a tumor cells (figure 4B). Protein expression levels of c-myc, n-myc and PD-L1 in Neuro2a and B16 cells were also significantly decreased following Myc targeting (figure 4C). Morphological changes of differentiation marked by dendrite production was also observed in the myc-inhibited cells compared with the untreated control cells[23] (figure 4D). Nestin, correlates with aggressiveness and stemness of cancer cells[24 25] and immunofluorescent staining showed it to be inhibited by Myc targeting in the Neuro2a cells figure 4E. Furthermore, treatment of both cancer cells with I-BET726/JQ1 led to a significant reduction in cell growth relative to untreated control (control

cells increased from 0.5×10^6 to 16×10^6 during 4 days of culture, while Myc inhibitor treated cells proliferated from 0.5×10^6 to 5×10^6). Trypan blue staining and microscopic observation revealed that the inhibitors did not compromise cell survival. Cell cycle was analyzed by Brdu-APC/7AAD staining and flow cytometry analysis showed that I-BET726 and JQ1 treatment arrested the majority of cells in the G0–G1 phase of cell cycle, and induced an enhancement of apoptosis (figure 4F).

In order to evaluate whether this bromodomain inhibitor approach is translatable to human neuroblastoma cells, we evaluated the effect of I-BET726 and JQ1 on MYCN suppression in four human neuroblastoma cell lines, SK-N-SH and SK-N-F1 (MYCN-non-amplified cell lines) and IMR32 and BE(2)C, (MYCN-amplified cell lines). All cells were exposed
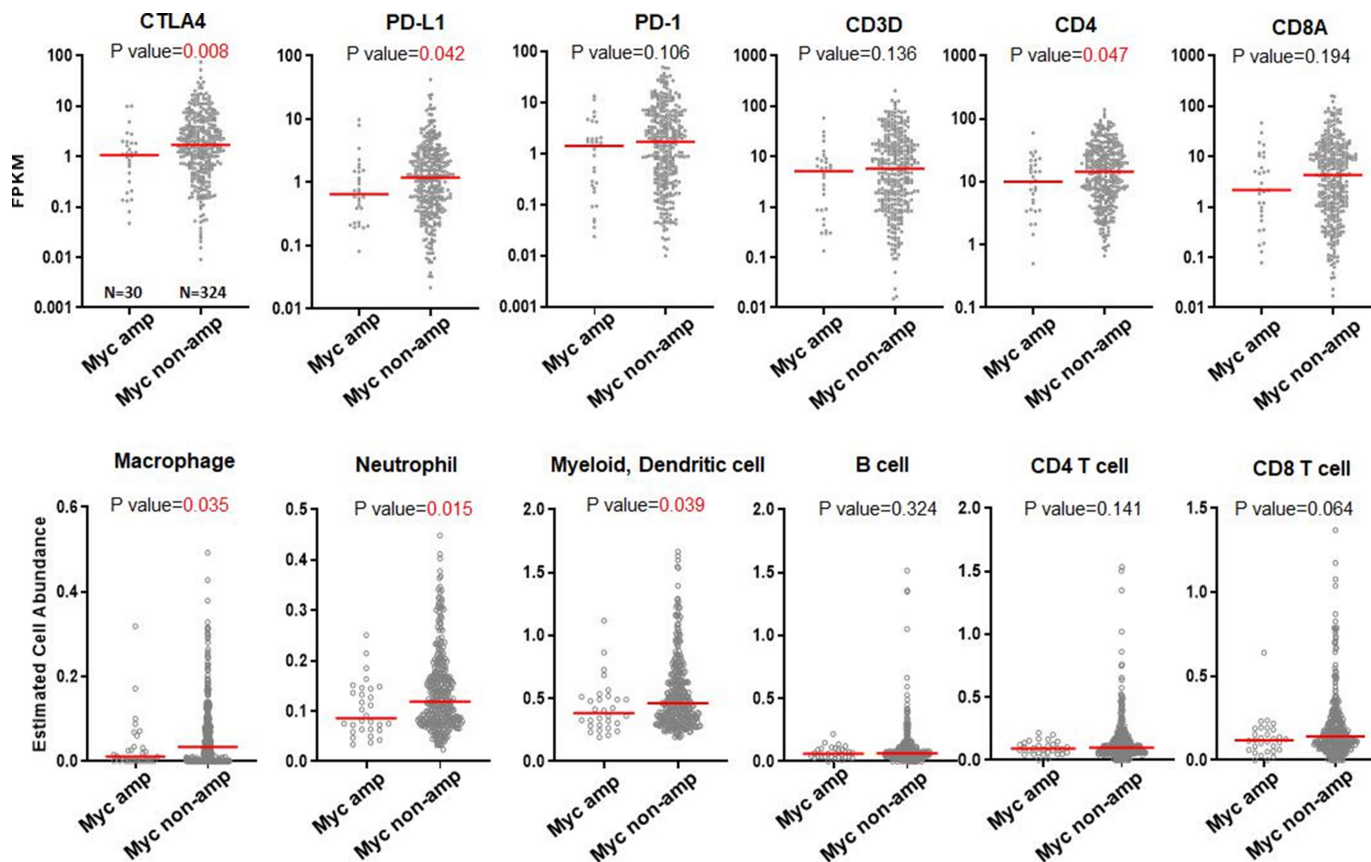
Figure 3 c-MYC amplification in melanoma affects immune gene expression and inflammatory immune cell phenotypes. The box plots showing the copies of the CTLA-4, PD-L1 and CD4 T cell transcripts are significantly decreased in Myc-amplified melanoma tumor samples (upper row). The estimated cell abundance of macrophages, neutrophils and myeloid DCs was significantly reduced in Myc-amplified tumors than in Myc non-amplified tumors (lower row). The solid red line means median value. Significance (p value) was determined by the Wilcoxon rank-sum test. Estimated immune cell abundance was calculated by timer algorithm. Statistically significant differences between the groups (p<0.05). DCs, dendritic cells; PD-L1, programmed death-ligand 1.

to different concentrations and/or combinations of I-BET726 and JQ1 and assessed at 3, 4, 5, 7 and 10 days. The gene expression and protein expression of MYCN, c-MYC and PD-L1 were determined with qPCR and western blotting and select blots are demonstrated in figure 4G, H and I. In baseline untreated conditions, BE(2)C has the highest MYCN expression and is followed by IMR32. MYCN was not expressed in SK-N-SH and minimally expressed in SK-N-F1 which are non-MYCN-amplified cell lines. Interestingly, the higher the MYCN expression, the lower the PD-L1 and c-MYC expression in these cell lines. Nevertheless, both western blotting and qPCR results demonstrated that the combination of I-BET726 and JQ1 produced suppression of MYCN and PD-L1 in all four human neuroblastoma cell lines (figure 4G and I). The optimal treatment for downregulating genes of interest in SK-N-SH is 1.5 μM for 3 days, 1 μM for 3 days in SK-N-F1, 2.5 μM for 3 days in BE(2)C and 0.25 μM for 5 days in IMR32. These results suggest that bromodomain inhibition of MYCN in human neuroblastoma cell lines is feasible and lays the groundwork for these preclinical findings to have potential clinical impact.

Myc inhibition induces tumor cell immunogenicity

To investigate the influence of downregulating Myc on tumor cell immunogenicity, an Interferon gamma IFNγ secretion assay was performed. I-BET726 and JQ1-treated N2a cells or B16 cells (with or without irradiation) and untreated cells were cocultured with syngeneic A/J or C57BL/6 splenocytes and IFNγ production was quantified at 24 hours and 48 hours by ELISA. Splenocytes produced significantly higher levels of IFNγ when they were cocultured with myc inhibitor-treated N2a cells as in figure 5A cells as in figure 5B. In addition to IFNγ, we also quantified other cytokine/chemokines using ProcartaPlex multiplex immunoassay in B16 cells. Thirteen out of 23 detectable cytokines were significantly upregulated when splenocytes were cocultured with myc-inhibited B16 tumor cells, including effector cytokines IFNγ, TNFα; stimulator cytokines, IL-18, G-CSF; inflammatory factors: IL-6; chemo attractive factors: CCL-5 (rantes), CXCL-1, CCL-2, CCL-7, CXCL-2, CCL3; and regulatory molecule: IL-10, (p<0.05, online supplemental figure 1). These findings show that Myc-inhibited tumor cells stimulate host immunity.
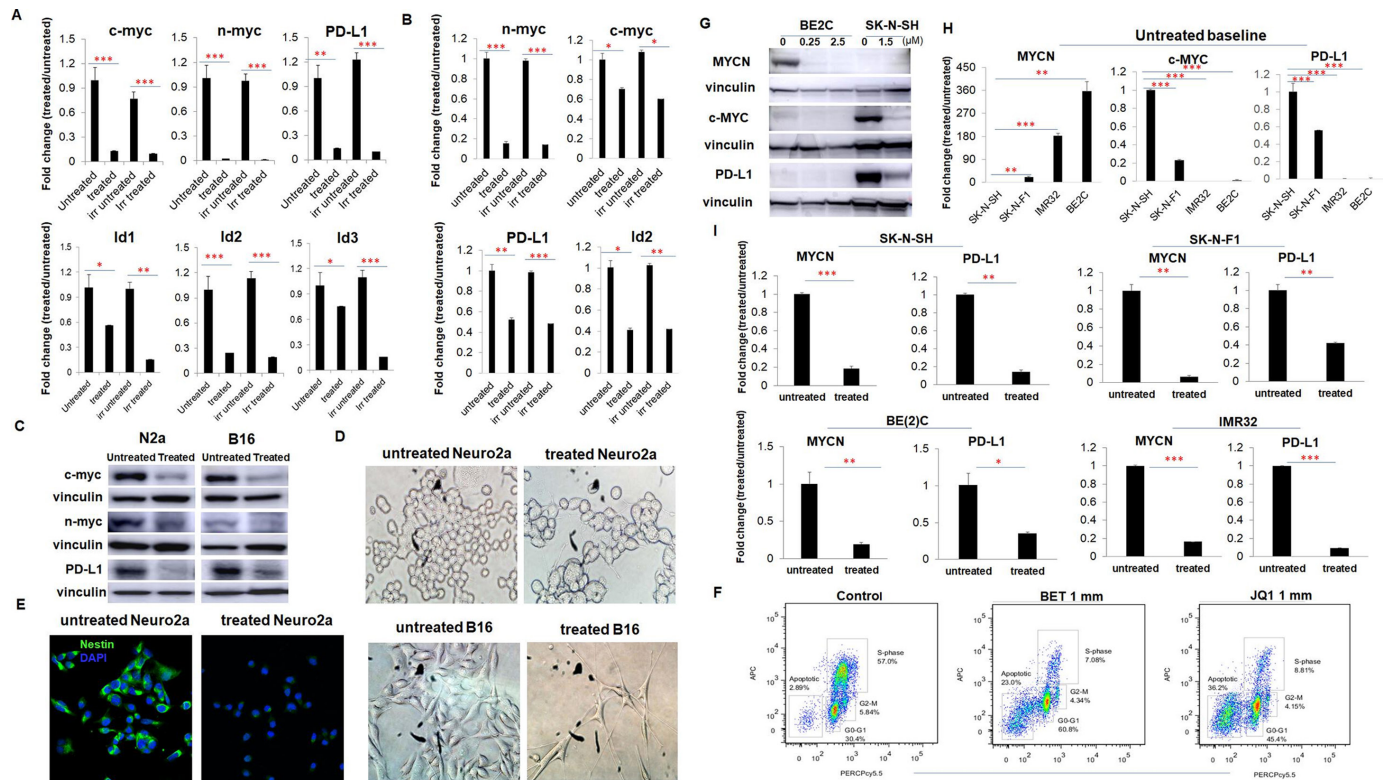
Figure 4 Combination BET and JQ1 treatment suppresses myc oncogene in melanoma B16 cells and neuroblastoma Neuro2a cells. (A, B) B16 cells and Neuro2a cells were treated with (0.25 µM) BET and (0.25 µM) JQ1 for 4 days, the mRNA expression of c-myc, N-myc, PD-L1 and ID genes in B16 cells and Neuro2a cells were determined by real-time qRT-PCR. Gene expression before and after irradiation (60 Gy) were compared for each gene as well. (C) The protein expression of c-myc in B16 cells and N-myc in Neuro2a cells were determined by western blotting. GAPDH was used as an internal control for both qPCR and western blot. (D) Bright-field microscopy images and (E) fluorescence microscopic appearance of nestin staining (green: nestin, blue: DAPI, original magnification, ×400) showed morphologic changes of B16 and Neu2a cells induced by BET/JQ1 treatment. (F) Cell cycle progression of B16 cells following treatment were determined by flow cytometry. BET and JQ1 treatment induced an enhancement of apoptosis (sub-G0) and G0–G1 cell cycle arrest in B16 cells. (G) Human neuroblastoma MYCN-amplified BE(2)C cells and MYCN non-amplified SK-N-SH cells were treated with BET and JQ1 for 3 days, and protein expression of MYCN, c-myc and PD-L1 were determined by western blotting. Vinculin was used as an internal control. (H) The gene expression of the baseline untreated cells is shown. (I) MYCN-amplified BE(2)C and IMR32 cells and MYCN non-amplified SK-N-SH and SK-N-F1 cells were treated with BET and JQ1 and the mRNA expression of MYCN and PD-L1 in these four cell lines was quantified by real-time qRT-PCR. GAPDH was used as an internal control for qPCR. Data are representative of three independent experiments. Results are expressed as mean score ±SD. *p<0.05; **p<0.005; ***p<0.001, determined by unpaired two-tailed Student's t-test. BET, bromodomain and extra-terminal motif; PD-L1, programmed death-ligand 1.

In order to further characterize the mechanism by which Myc suppression leads to enhanced tumor cell immunogenicity, we compared Myc-targeted B16 cells with untreated B16 cells using NanoString Mouse PanCancer Immune Profiling analysis. Unsupervised clustering results in a complete separation of five treated samples from six untreated samples, showing the heat map of all genes in figure 5C. An overview of pathway score changes across samples is displayed in the heat map in figure 5D. The distribution of I-BET726/JQ1 treated cells is clustered tightly and shows an overall pattern of higher expression of immune-related genes/pathways than untreated samples. The top 20 statistically significantly altered genes are listed in online supplemental table S6. The scores of the immunological functions related to cytokine, chemokine, interleukin, interferon,

Major Histocompatability Complex (MHC), antigen processing, DC and CD molecule are significantly upregulated in treated cells and is shown in figure 5E. Taken together these results suggest that blockade of Myc oncogene in melanoma tumor cells significantly induces both functional and genotypic characteristics of immunogenicity and may be exploited as an antigen source for whole cell vaccination.

Myc-targeted whole tumor cell vaccination induced tumor immunity in mouse neuroblastoma and melanoma models

We tested the use of Myc-inhibited whole tumor cell vaccination in two therapeutic treatment mouse models (neuroblastoma and melanoma). 2×10^6 WT Neuro2a or 1×10^4 B16 melanoma cells were subcutaneously administered on day 0 on the right leg of AJ or C57Bl/6 mice, respectively and vaccination in each model was performed
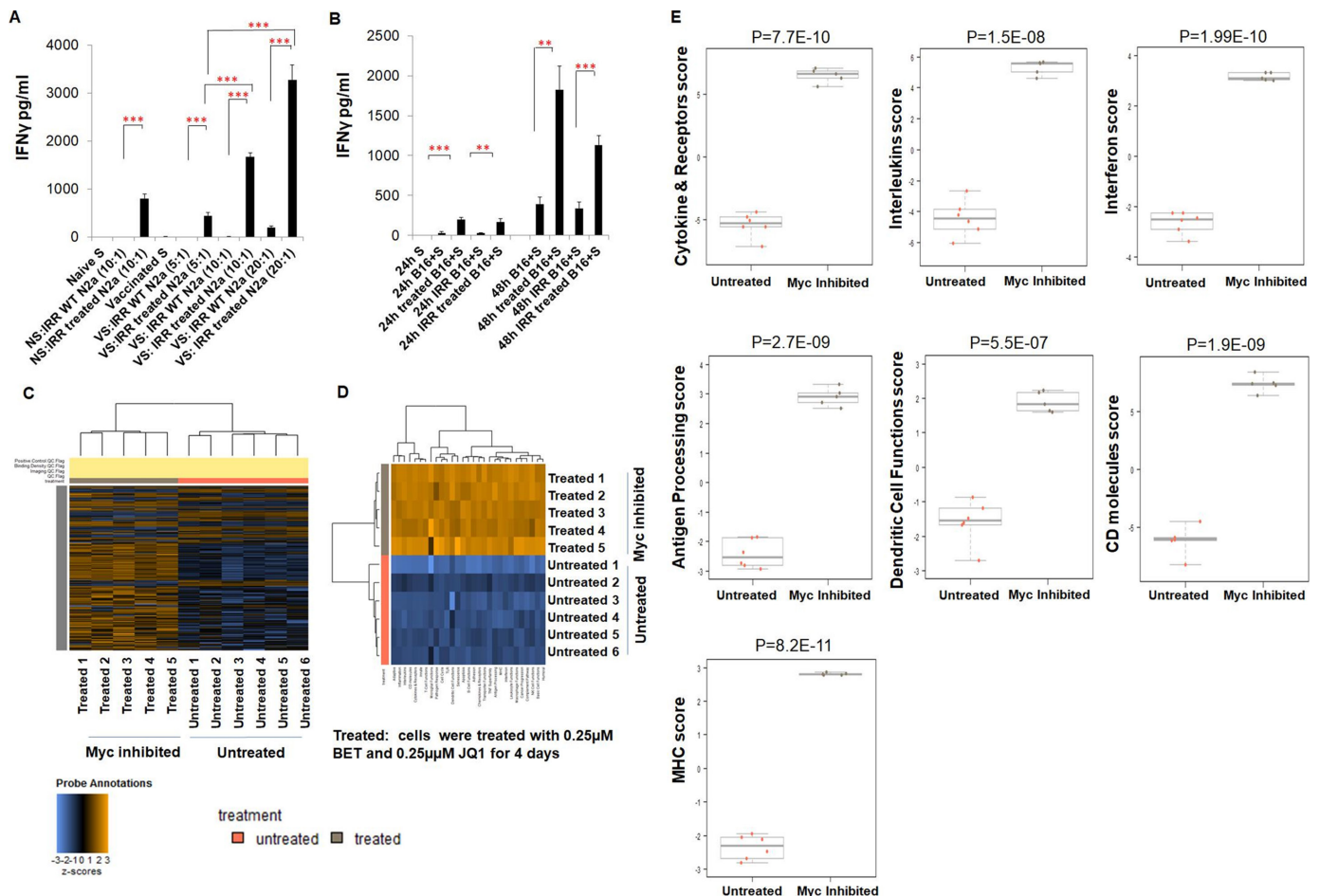
Figure 5 Inhibition of c-Myc expression in B16 melanoma cells enhances tumor cell immunogenicity. (A) IFNγ production from naive splenocytes in a tumor cell—splenocyte reaction. B16 cells were treated with BET (0.25 μM) and JQ1 (0.25 μM) for 4 days, and then these cells were irradiated (60 Gy). Treated (or untreated) B16 cells were cocultured with mouse naive splenocytes for 24 hours and 48 hours in a (1:10) ratio of effector cells to target cells. ELISA results show that IFNγ concentration in media was significantly increased when splenocytes were cocultured with treated B16 cells at two different time points. S: naive splenocytes; Irr: irradiated. (B) Heat map of differentially expressed immune genes in B16 cells following exposure to BET and JQ1 combination treatment using NanoString nCounter mouse PanCancer immune profiling. Colored horizontal bars along the top of the plot identify covariate categorizations. Orange: untreated samples (n=6); gray: treated samples (n=5). (C) Heat map of pathway scores. pathways are listed on the horizontal axis and samples are listed vertically. Orange indicates high scores; blue indicates low scores. (D) Pathway scores were presented as box plots for select immune pathways of interest. Data are representative of three independent experiments. Results are expressed as mean score ±SD. *p<0.05; **p<0.005; ***p<0.001, determined by unpaired two-tailed Student's t-test. BET, bromodomain and extra-terminal motif.

as described in the Methods section (figure 6A and G). Tumor growth and mouse longevity were monitored and compared (figure 6B–F and H–I). None of the mice developed tumor at the site of the vaccine cell injection. Significant therapeutic survival benefit was observed in both models, but was more profound in the neuroblastoma model. In the Neuro2a model, six of eight mice, 75% were cured of the high dose 7 day established tumors (figure 6B). Moreover, four out of these six mice that rejected tumor developed long-term immunity against a further WT tumor cell (2×10^6) rechallenge 2 months later (figure 6F). In the B16 model, the vaccine resulted in a significant delay in tumor growth in the vaccination group (62% survival at day 30) compared with the control unvaccinated mice (0% survival) and the checkpoint inhibitor alone group (14% survival) in the 4-day

established melanoma tumor model (figure 6H). The average tumor size was significantly smaller in the vaccinated group (n=13) compared with both unvaccinated controls (p<0.001, n=16), and checkpoint inhibitor only (p<0.05, n=7) at day 22, when mice were euthanized due to the end-point of tumor size (20 mm^3, figure 6I). The findings suggest that small molecule suppression of Myc renders tumor cells immunogenic and presents an opportunity to exploit cancer cells for therapeutic whole cell vaccination in the context of checkpoint inhibition. Of notable interest, we found this novel therapeutic vaccine to be remarkably more effective in the mouse neuroblastoma tumor model than in melanoma model.

Despite the improvement in survival and the slowed tumor growth in the melanoma model the failure to obtain cures, led us to further examine the phenotype
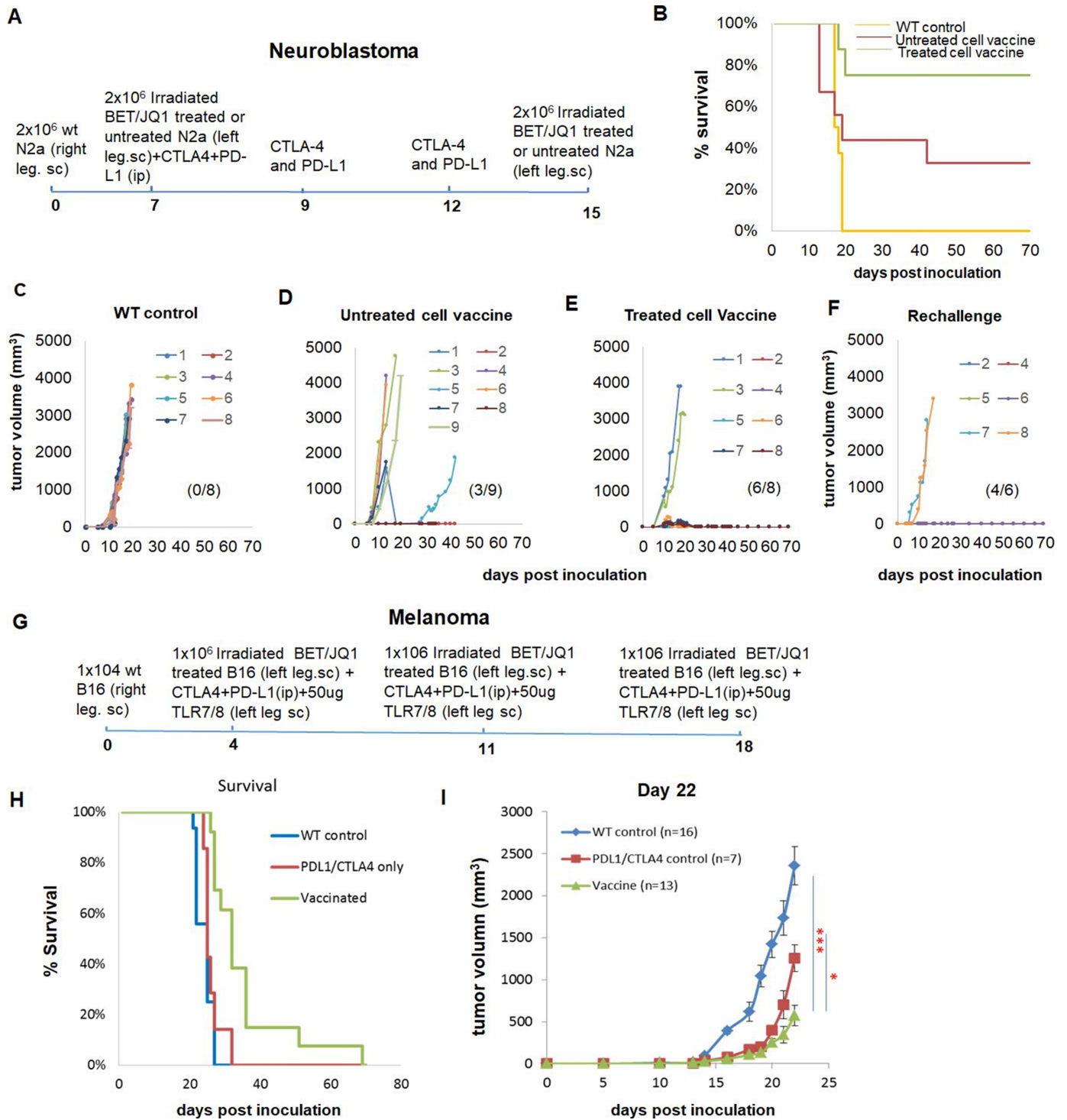
Figure 6 Vaccination with BET/JQ1-treated whole tumor cells improves outcome in both neuroblastoma and melanoma mouse tumor models. (A) The vaccination protocol and timeline for neuroblastoma model. (B) Survival curve of neuroblastoma model. (C, D, E) Individual tumor growth in various treatment groups of neuroblastoma model following vaccination. Six (75%) out of eight mice were cured of tumors when the MYC-targeted whole cell vaccine was combined with inhibition of CTLA-4 and PD-L1 checkpoints, whereas all mice challenged with wt Neuro2a (wt control, n=8) died from tumor burden and six of nine mice died of tumor burden when vaccinated with irradiated untreated Neuro2a and checkpoint inhibition (33% cure rate). Cure rate is in parenthesis. (F) The tumor-free mice from (D) (n=6) were rechallenged with 2×10^6 wtN2a cells into their left leg and four out of six (67%) were immunized against wt tumor growth. (G) The vaccination protocol and timeline for the melanoma model. (H) Survival curve of melanoma model. (I) Average melanoma tumor growth curves with differences in growth curves. Data are representative of three independent experiments. Error bars indicate SD. *p<0.05, **p<0.01; ***p<0.001, determined by Student's t-test. BET, bromodomain and extra-terminal motif; PD-L1, programmed death-ligand 1; WT, wild-type.

and kinetics of immunity following vaccination. We evaluated melanoma TILs from dissociated tumor, spleen, tumor-draining inguinal lymph nodes (TLN) and contralateral lymph nodes (CLN) with flow cytometry. To ensure that mice would have tumors at the time of evaluation, we started treatment 7 days after tumor cell inoculation (instead of day 4), and provided three doses of vaccination on day 7, 10 and 13 with the two checkpoint inhibitors (CTLA-4 and PD-L1). Mice were euthanized on day 15 and day 22, when tumors reached about 5 mm and 12 mm in one dimension. Our results demonstrated that the population of total lymphocytes (CD45$^+$ cells), cytotoxic T cells (CD8α^+ cells), proliferating cytotoxic T cells

(Ki67$^+$CD8α^+ cells), T helper (CD4$^+$Foxp3$^-$ cells) and CD8$^+$CD11C$^+$ DCs, are all significantly increased in the tumors that were collected from vaccinated mice on day 15 and day 22 following inoculation of wt B16 tumor cells compared with tumors from untreated mice (figure 7A). A significant increase of proliferating cytotoxic T cells (CD8$^+$Ki67$^+$), CD8$^+$CD11C$^+$ DCs and CD4$^+$FoxP3$^-$ T helpers was also observed in the TLN, CLN and spleen at day 15. These enhancements did not persist at day 22. Given that a higher cytotoxic to regulatory T-cell ratio (CD8α^+/FoxP3$^+$) and lower ratio of T helper/regulatory T cells (Treg) is previously shown to signify favorable
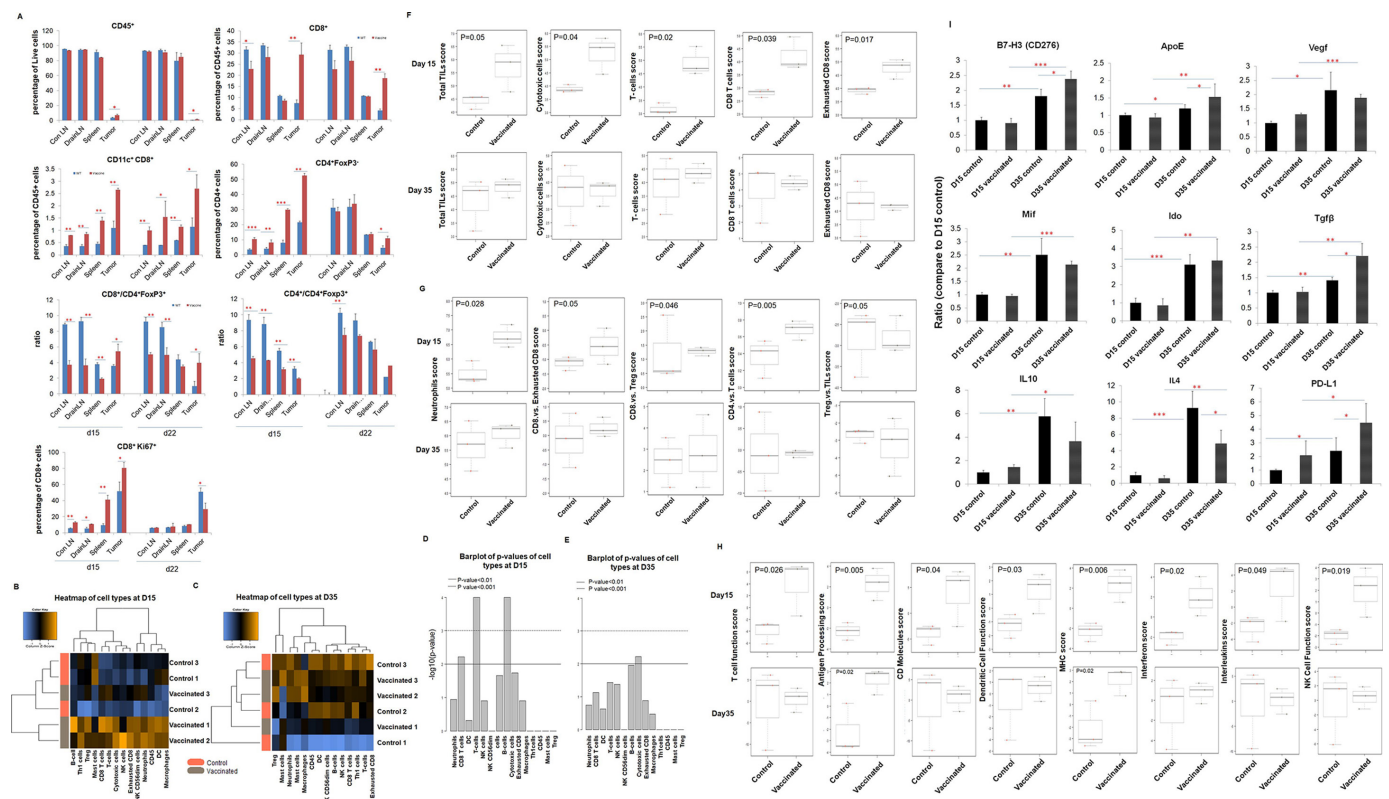
Figure 7 The combination of cancer vaccination and checkpoint inhibitors enhances infiltration of immune cells into mouse melanoma tumors at day 15, but not at the tumor endpoint of day 35 compared with unvaccinated controls. (A) Tumor, spleen, TLNs and CLNs from vaccinated and unvaccinated mice were stained with specific mAbs and analyzed by flow cytometry at day 15. The relevant isotype control sample was set as negative control. The bars represent means±SD. *p<0.05, **p<0.01; ***p<0.001 versus control (n=3 tests for each group). (B) Heat map of cell type measurements from vaccinated tumor (n=3) versus unvaccinated tumor tissues (n=3) at day 15 and then at endpoint day 35. (C) Showing the abundance of different cell types. Cell types are listed on the horizontal axis and samples are listed vertically. orange indicates high abundance, whereas blue indicates low abundance. (D) Bar plot of p values of immune cell types from tumors at day 15 and (E) at endpoint day 35 (p values are −log10 transformed). Bars above the solid black line indicates cell types that are significantly different at a p value 0.01 (vaccinated vs unvaccinated tumor). Bars above the dashed black line indicate significance at a p value threshold of 0.001. (F) Bar plots representing T-cell type and function score comparison between vaccinated and unvaccinated tumors at day 15 and day 35. The bars represent means±SD (p values of vaccinated vs control). The significant increases in immune cell scores noted at day 15 were absent at the tumor endpoint day 35. (G) Bar plots representing: TILs, neutrophils, CD8 to Treg score and CD4 to Treg score. Again, the significant increases in immune cell scores noted at day 15 were absent at the tumor endpoint. (H) Similarly, bar plots of functional and antigen processing scores at day 15 and day 35. (I) Bar plots of suppressive immune molecules in tumors of control and vaccinated mice at day 15 and day 35. Note the significant increase in all immune suppressor molecules as the tumors grow in both control and vaccinated mouse models favoring immune resistance. Data are representative of three independent experiments. *p<0.05, **p<0.01; ***p<0.001, determined by Student's t-test. CLNs, contralateral lymph nodes; mAbs, monoclonal antibodies; TILs, tumor infiltrating lymphocytes; TLNs, tumor-draining lymph nodes; Treg, regulatory T cells.

outcomes in several cancer types,[26 27] we measured these cell ratios after vaccination. The ratio of CD8α⁺ cell/CD4⁺ Foxp3⁺ cells was significantly increased and the ratio of CD4⁺FoxP3⁻cell/CD4⁺FoxP3⁺ cells was significantly decreased in tumor tissue from the vaccination group. Interestingly, the ratio of CD8α⁺ cell/CD4⁺ Foxp3⁺ cells was significantly decreased in CLN, TLN and spleen at both day 15 and day 22 in vaccinated mice, which could be due to the massive influx of CD8α⁺ cells into tumor from these locations. We also quantified monocytes (CD11b⁺GR1⁺), mature NK cells (DX5⁺), macrophages (F4/80⁺CD11b⁺) and Treg (CD4⁺FoxP3⁺). The data are shown in online supplemental figure 2, in which no significant change in these immune cell phenotypes is observed.

To further dissect the profile and kinetics of immune cells infiltrating the tumor microenvironment and to identify potential mechanisms of therapeutic resistance in the melanoma model, we investigated the global expression of mRNA isolated from vaccinated (n=3) and unvaccinated (n=3) tumors at day 15 and at the end time point, day 35 using NanoString PanCancer Immune Profiling arrays (figure 7B–7H). At day 15, we observed a profound and statistically significant increase in the expression of signature markers for total TIL, T cells, cytotoxic cells, CD8⁺ T cells, exhausted CD8⁺ cells, and neutrophils in the tumors from vaccinated groups (figure 7D and F). Moderate but statistically significant differences of the relative expression of CD8⁺ effector T cells versus exhausted CD8⁺ T cells, CD8⁺ T cells versus Treg cells and CD8⁺ effector T cells versus total TIL cells were also observed in the vaccinated group versus unvaccinated group (representative graphs are shown in figure 7G). In addition, multiple immune pathway scores including antigen processing, CD molecule, interferon, interleukin, MHC, DC function, NK cell function, T cell function were all significantly enhanced in the vaccinated group (figure 7H). These enhanced immunogenic profile patterns are consistent with the results of the flow cytometry analysis of cell type frequency shown in figure 7A. This data suggest that the combination of cancer vaccination and checkpoint inhibitors enhances infiltration of immune cells into the tumor microenvironment. However, when comparing gene expression profile results between vaccinated and unvaccinated mice at the end point (day 35; tumor size 20 mm in one diameter), we did not find improvement in most of the immune cell scores or the immune pathway scores in the vaccinated group. Exceptions proved to be antigen processing and MHC pathway scores. These two pathway are significantly increased in the vaccination group, but their p values are more significant at day 15, suggesting a progressive mechanism of therapeutic resistance (figure 7C, E, F, G and H). Nanostring analysis also demonstrated an overproduction of negative modulators of immune function, including macrophage migration inhibitory factor, transforming growth factor-β (TGF-β), vascular endothelial growth factor (VEGF), ApoE, indolamine 2,3-dioxygenase

(IDO), PD-L1 and B7-H3 that progressively increased with continued tumor growth. Inhibitory signals IL-10 and IL-4 also increased significantly (figure 7I). These changes could explain the adaptive resistance gained by the tumor that is associated with an imbalance between tumor cell growth and cytotoxic killing and thus a failure of the vaccine to eradicate the tumor in the melanoma model.

DISCUSSION/CONCLUSION

Amplification or overexpression of the MYC oncogene is a well-established and frequent event in many malignancies including neuroblastoma and melanoma. The exact role of c-Myc and MYCN in the respective tumors is uncertain, but our findings show that both are associated with immune suppression. MYCN amplification is associated with risk stratification in neuroblastoma in which high-risk disease and increased mortality is a well-defined association with amplification.[19 28–30] In tumorigenesis MYC enhances cell proliferation and angiogenesis, and inhibits cellular differentiation. New evidence suggests that Myc is also associated with tumor immunosuppression by altering expression of immunity genes.[3 31] In this study, amplification of MYCN in neuroblastoma was associated with remarkable suppression of tumor immunity pathways, supporting our earlier study.[1] Suppression is especially evident in genes involved in T cell function and cytotoxicity, mechanisms critical for effective immunotherapy. It is also of note that c-MYC amplification in the melanoma in silico study we analyzed was also associated with suppression of immune cell infiltrates.

In addition to showing that MYC suppresses interferon and proinflammatory pathway activity and leads to a T-cell/cytotoxic poor microenvironment, we also found that MYCN amplification leads to decreased expression of immunosuppressive genes in neuroblastoma cells, such as ANXA1, CD73 (NT5E), AXL, APOE, VEGF and PD-L1 and the loss of antigen presentation and processing genes, such as MHC-I (HLA-A, HLA-B, HLA-C), MHC-II (HLA-DP, HLA-DR) and TAP molecules (TAP1, TAP2, TAPBP). Two more genes PMSB9 (161-fold downregulated, p value=0.001) and THBS1 (273-fold downregulated, p value=7.88E−06) are also of interest. PSMB9 is involved in degradation machinery of antigens that enables presentation of the resulting peptides to cytotoxic T lymphocytes.[32 33] THBS1 is the transporter associated with antigen processing for MHC-I and interacts with the CD47 'don't eat me' signal, and is a potent inhibitor of T cell and DC activation.[34–36] Major cancer testis (CT) antigens are also downregulated more than 100 fold (p value <0.001) with MYCN amplification which are prime antigen targets for host T-cell responses. It is of interest to note that all immune pathways are suppressed with MYC amplification, which may speak to the lack of tumor immunogenicity and thus the redundancy for immune evasive or tumor protective mechanisms. The paucity of intratumoral T cells and lower PD-L1 expression before

treatment is shown to predict poor responses to checkpoint inhibitors in other tumors[37] and clinical trials that have evaluated checkpoint blockade immunotherapy alone in patients with high-risk neuroblastoma, have not been successful.[4] Paradoxically, from an immunotherapeutic perspective a lack of immunogenicity may offer an opportunity to target those tumors that would be less resistant to host immunity assuming potent cellular immunity can be generated against the tumor. This phenomenon could have important implications for vaccine therapy of non-immunogenic high-risk disease. We have previously described this phenomenon in neuroblastoma, but it was also observed in the RNAseq data we obtained from patients with melanoma, in that cMYC-amplified tumors expressed lower levels of PD-L1 and CTLA4 than non-amplified tumors.

In our analysis of human neuroblastoma cell lines, we found an association with immunesuppressive phenotype and MYCN amplification. The validity of immune profiling cell lines that have been maintained for years in vitro without any immunologic pressure must be questioned. However, despite this artificial culture environment, the cell lines show remarkable innate differences in genes and pathways of immunity reiterating the close association with MYCN amplification and a non-immunogenic phenotype. This association reflects the intrinsic effect of MYCN amplification on tumor cell immunity as opposed to the extrinsic pressure of the host environment.

Based on these findings, we targeted Myc in tumor cells with the goal of improving the immune-stimulatory capacity of whole cell vaccines when combined with checkpoint inhibition. This strategy could enable tumor antigen presentation and T-cell priming to establish tumor immunity and evoke long-lasting immune memory for tumor cell elimination in patients underserved by current therapies. To develop this vaccine, we first targeted Myc gene expression in both mouse neuroblastoma and melanoma cell lines with small molecule Myc inhibitors. Myc is a transcription factor that was considered a poor drug target, until recent approaches suggested that downregulation of Myc is possible by indirect targeting using bromodomain and extra-terminal motif (BET) inhibitors. We tested for the effects of different doses, drug combinations and incubation times on tumor cell proliferation, differentiation and gene alteration. We found that combination $0.25\,\mu M$ BET726 plus $0.25\,\mu M$ JQ1 treatment for 4 days had the most consistent effect on Myc depletion and phenotypic induction of differentiation and used this combination as a standard to develop our mouse tumor cell vaccines. These treated cancer cells were strongly immunogenic in both functional and phenotypic assays producing molecules and stimulatory mechanisms critical for activating both innate and acquired immunity and overcoming T-cell anergy.

We studied two models to evaluate the Myc-targeted cell lines as whole cell vaccines in combination with checkpoint inhibitors. Our data in two primary tumor models are quite different, which emphasizes the value

of studying more than one mouse model. Although both tumors arise from neural crest origin, they are remarkably different in their response to immunotherapy. We believe our data define the difference in immune-suppressive molecules protecting the melanoma against induced immunity. In the neuroblastoma model, combination of both vaccination and checkpoint inhibitors resulted in a 75% cure and significantly improved long-term survival despite a larger initial tumor challenge. Sixty-seven per cent of mice that rejected the initial tumor survived a rechallenge, indicating long-term immune memory. In contrast, the same tumor vaccination strategy in the melanoma mouse model induced only partial immunity against a lesser tumor cell challenge. The vaccine produced significant immune cell infiltrates in tumors following vaccination. A large influx of activated CD8+ cytotoxic T cells, CD4+ helper T cells, DC, neutrophil and NK cells appeared in tumors after vaccination, with a simultaneous decrease in the number of Treg cells. Despite the potent favorable cellular and molecular changes of tumor immunity in the vaccinated melanoma mice, these significant changes were still inadequate to cure mice of their tumors. The observation of failure to cure may be explained in these mice, by upregulation of suppressive molecules as the tumors continued to grow despite an abundant infiltration of antitumor cellular immunity. Molecules of significant interest include the upregulation of PD-L1, ApoE, VEGFa, TGFb1, CD276, CD74, IDO, IL-10, IL-4 and CXCL15. Despite attempting to block PD-L1 and CTLA-4, the therapeutic effect could well be hindered by incomplete blockade and by many of these other suppressive molecules. Further identifying and targeting key pathways from this group of suppressive molecules is our next priority.

Translating our findings to patient care will necessitate the ability to generate cell lines from a patient's own tumor. Conceptually at the time of initial tumor biopsy at diagnosis, we envision harvesting tumor cells and developing a patient-specific tumor cell line. In the case of neuroblastoma, the patient would then undergo the standard treatment for neuroblastoma which entails about 12 weeks of therapy. Once the patient is in a state of minimal residual disease, the patient's established tumor cell line will be subjected to MYC-targeted treatment in a Good Manufacturing Practice facility and prepared for irradiation and subsequent whole cell vaccination combined with checkpoint inhibition therapy. A potential weakness of this protocol would be the inability to establish a cell line, but the high-risk neuroblastoma tumors for which this therapy would be ideally suited are more easily established due to their aggressive behavioral phenotype.

In conclusion, our studies reiterate the important association between neuroblastoma MYCN oncogene amplification and immunosuppression in the tumor microenvironment. Similarly, MYCN-amplified human cell lines have a non-immunogenic profile, while MYCN non-amplified cells appear to have an immunogenic gene profile. We demonstrate that small molecule inhibitors

can potently suppress Myc expression and in so doing, enhance the immunogenicity of the tumor cells themselves, enabling their use as a whole cell tumor vaccine. This whole cell vaccine in combination with checkpoint inhibitors generates broad tumor-specific cellular immunity against both mouse neuroblastoma and melanoma tumors. Despite these potent effects, other immunosuppressive molecules will need to be targeted to see the full effects of the vaccine protocol in the melanoma model. Most importantly, our work provides the framework and rationale for translation of our findings into a therapeutic patient-specific vaccine for MYCN-amplified neuroblastoma tumors resistant to available therapies.

Author affiliations
[1]The Sheikh Zayed Institute for Pediatric Surgical Innovation, Childrens Hospital Medical Center, Washington, District of Columbia, USA
[2]Center for Cancer and Immunology Research, Children's National Hospital, Washington, DC, USA
[3]Division of Immunotherapy, Institute of Human Virology, University of Maryland School of Medicine, Baltimore, Maryland, USA
[4]Joseph E. Robert Jr. Center for Surgical Care, Childrens National Hospital, Washington, District of Columbia, USA

ORCID iDs
Xiaofang Wu http://orcid.org/0000-0002-3782-7701
Anthony David Sandler http://orcid.org/0000-0001-9440-2964

REFERENCES

1 Zhang P, Wu X, Basu M, et al. MYCN Amplification Is Associated with Repressed Cellular Immunity in Neuroblastoma: An In Silico Immunological Analysis of TARGET Database. Front Immunol 2017;8:1473.
2 Srinivasan P, Wu X, Basu M, et al. Pd-L1 checkpoint inhibition and anti-CTLA-4 whole tumor cell vaccination counter adaptive immune resistance: a mouse neuroblastoma model that mimics human disease. PLoS Med 2018;15:e1002497.
3 Layer JP, Kronmüller MT, Quast T, et al. Amplification of N-myc is associated with a T-cell-poor microenvironment in metastatic neuroblastoma restraining interferon pathway activity and chemokine expression. Oncoimmunology 2017;6:e1320626.
4 Anderson J. Unleashing the immune response against childhood solid cancers. Pediatr Blood Cancer 2017;64. doi:10.1002/pbc.26548. [Epub ahead of print: 06 Apr 2017].
5 Dang CV. Myc on the path to cancer. Cell 2012;149:22–35.
6 Müller I, Larsson K, Frenzel A, et al. Targeting the MYCN protein with small molecule c-myc inhibitors. PLoS One 2014;9:e97285.
7 Delmore JE, Issa GC, Lemieux ME, et al. Bet bromodomain inhibition as a therapeutic strategy to target c-myc. Cell 2011;146:904–17.
8 Choi SK, Hong SH, Kim HS, et al. Jq1, an inhibitor of the epigenetic reader BRD4, suppresses the bidirectional MYC-AP4 axis via multiple mechanisms. Oncol Rep 2016;35:1186–94.
9 Wyce A, Ganji G, Smitheman KN, et al. Bet inhibition silences expression of MYCN and Bcl2 and induces cytotoxicity in neuroblastoma tumor models. PLoS One 2013;8:e72967.
10 Pan Y, Fei Q, Xiong P, et al. Synergistic inhibition of pancreatic cancer with anti-PD-L1 and c-myc inhibitor JQ1. Oncoimmunology 2019;8:e1581529.
11 Mertz JA, Conery AR, Bryant BM, et al. Targeting Myc dependence in cancer by inhibiting BET bromodomains. Proc Natl Acad Sci U S A 2011;108:16669–74.
12 Filippakopoulos P, Qi J, Picaud S, et al. Selective inhibition of BET bromodomains. Nature 2010;468:1067–73.
13 Fowler T, Ghatak P, Price DH, et al. Regulation of Myc expression and differential JQ1 sensitivity in cancer cells. PLoS One 2014;9:e87003.
14 Posternak V, Cole MD. Strategically targeting Myc in cancer. F1000Res 2016;5. doi:10.12688/f1000research.7879.1. [Epub ahead of print: 29 Mar 2016].
15 Wu S-Y, Chiang C-M. The double bromodomain-containing chromatin adaptor Brd4 and transcriptional regulation. J Biol Chem 2007;282:13141–5.
16 Cesano A. nCounter(®) PanCancer Immune Profiling Panel (NanoString Technologies, Inc., Seattle, WA). J Immunother Cancer 2015;3:42.
17 Danaher P, Warren S, Dennis L, et al. Gene expression markers of tumor infiltrating leukocytes. J Immunother Cancer 2017;5:18.
18 Chakrabarti L, Abou-Antoun T, Vukmanovic S, et al. Reversible adaptive plasticity: a mechanism for neuroblastoma cell heterogeneity and chemo-resistance. Front Oncol 2012;2:82.
19 Huang M, Weiss WA. Neuroblastoma and MYCN. Cold Spring Harb Perspect Med 2013;3:a014415.
20 Valentijn LJ, Koster J, Haneveld F, et al. Functional MYCN signature predicts outcome of neuroblastoma irrespective of MYCN amplification. Proc Natl Acad Sci U S A 2012;109:19190–5.
21 Zhu H, Bengsch F, Svoronos N, et al. Bet bromodomain inhibition promotes anti-tumor immunity by suppressing PD-L1 expression. Cell Rep 2016;16:2829–37.
22 Ohashi K, Kobayashi G, Fang S, et al. Surgical excision combined with autologous whole tumor cell vaccination is an effective therapy for murine neuroblastoma. J Pediatr Surg 2006;41:1361–8.
23 Steingrímsson E, Copeland NG, Jenkins NA. Melanocyte stem cell maintenance and hair graying. Cell 2005;121:9–12.
24 Ishiwata T. Cancer stem cells and epithelial-mesenchymal transition: novel therapeutic targets for cancer. Pathol Int 2016;66:601–8.
25 Narita K, Matsuda Y, Seike M, et al. Nestin regulates proliferation, migration, invasion and stemness of lung adenocarcinoma. Int J Oncol 2014;44:1118–30.

26 Shen Z, Zhou S, Wang Y, *et al*. Higher intratumoral infiltrated Foxp3+ Treg numbers and Foxp3+/CD8+ ratio are associated with adverse prognosis in resectable gastric cancer. *J Cancer Res Clin Oncol* 2010;136:1585–95.

27 Yao X, Ahmadzadeh M, Lu Y-C, *et al*. Levels of peripheral CD4(+) FoxP3(+) regulatory T cells are negatively associated with clinical response to adoptive immunotherapy of human cancer. *Blood* 2012;119:5688–96.

28 Brodeur GM, Seeger RC, Schwab M, *et al*. Amplification of N-myc in untreated human neuroblastomas correlates with advanced disease stage. *Science* 1984;224:1121–4.

29 Seeger RC, Brodeur GM, Sather H, *et al*. Association of multiple copies of the N-myc oncogene with rapid progression of neuroblastomas. *N Engl J Med* 1985;313:1111–6.

30 Davidoff AM. Neuroblastoma. *Semin Pediatr Surg* 2012;21:2–14.

31 Casey SC, Baylot V, Felsher DW. The Myc oncogene is a global regulator of the immune response. *Blood* 2018;131:2007–15.

32 Huang M, Zhang W, Guo J, *et al*. Improved transgenic mouse model for studying HLA class I antigen presentation. *Sci Rep* 2016;6:33612.

33 Ferrington DA, Gregerson DS. Immunoproteasomes: structure, function, and antigen presentation. *Prog Mol Biol Transl Sci* 2012;109:75–112.

34 Vallejo AN, Mügge LO, Klimiuk PA, *et al*. Central role of thrombospondin-1 in the activation and clonal expansion of inflammatory T cells. *J Immunol* 2000;164:2947–54.

35 Feliz-Mosquea YR, Christensen AA, Wilson AS, *et al*. Combination of anthracyclines and anti-CD47 therapy inhibit invasive breast cancer growth while preventing cardiac toxicity by regulation of autophagy. *Breast Cancer Res Treat* 2018;172:69–82.

36 Roberts DD, Kaur S, Soto-Pantoja DR. Therapeutic targeting of the thrombospondin-1 receptor CD47 to treat liver cancer. *J Cell Commun Signal* 2015;9:101–2.

37 Havel JJ, Chowell D, Chan TA. The evolving landscape of biomarkers for checkpoint inhibitor immunotherapy. *Nat Rev Cancer* 2019;19:133–50.